Relativistic dynamics of electrons in intense laser fields

J. N. Bardsley and B. M. Penetrante
Lawrence Livermore National Laboratory, Livermore, California 94550

M. H. Mittleman
City College of the City University of New York, New York, New York 10031
(Received 2 May 1989)

Following a brief review of the analytic solution for the relativistic motion of a single electron in a pulse of very strong plane-wave radiation, numerical simulations are presented that probe the effects of space-charge forces and spatial inhomogeneity of the radiation upon the one-electron dynamics. The nonlinearities introduced by relativistic effects can lead to irregular dynamics. For pulses with a smoothly varying temporal envelope the behavior of electrons that are ionized during the pulse can be very different from that of ambient electrons. The calculations support the use of short-pulsed lasers to produce high-energy electrons and incoherent x rays, but reveal possible difficulties in the formation of cold overionized plasmas suitable for recombination lasers.

I. INTRODUCTION

Interest in the interaction of atoms with intense electromagnetic radiation has been stimulated by the recent development of short-pulse lasers that can be focused to spot sizes of only a few times the laser wavelength. Intensities of over 10^{16} W/cm^2 have been achieved in several laboratories[1-3] and equipment has been designed to provide $10^{19}-10^{21}$ W/cm^2. In such fields light atoms will be completely stripped and heavy atoms will lose many of their electrons. The natural frequencies of the remaining electrons are very high compared with the frequency of the lasers in current use, so that high-field ionization rates depend very weakly upon frequency and can be estimated from dc tunneling rates.[4] Many of the subtleties of multiphoton ionization may thus disappear at very high intensities.

It is now well established that photoelectrons can absorb many more than the minimum number of laser photons required for ionization and can emerge from the focal region of the laser with considerably energy. Corkum, Burnett, and Brunel[5] have developed a quasiclassical model for the energy spectrum of photoelectrons. First the electron is detached from the atom, thereby absorbing the ionization potential, and then it interacts in a classical fashion with the fluctuating laser field. The probability for the initial ionization is obtained from dc ionization theory, with a field strength equal to the instantaneous field value. With linearly polarized light, the electrons will be emitted preferentially at those points in the optical cycle at which the field is near its maximum value, whereas for circularly polarized light there will be no preferred times for emission during each cycle. Corkum *et al.*[5] have analyzed the dynamics of the photoelectrons after their release from the atoms and have shown that the two modes of polarization lead to very different energy distributions for the electrons as they emerge from the strong-field region.

For laser intensities above 10^{19} W/cm^2 the dynamics of photoelectrons may become strongly relativistic. Boyer, Luk, and Rhodes[6] have pointed out that for Kr:F lasers at 10^{21} W/cm^2, the photoelectrons may reach energies in excess of 10 MeV and that laser-driven electrofission may be observable. At more modest intensities the production of a plasma with electron energies in the range of 10^3-10^6 eV could clearly lead to inner-shell ionization by electron impact that could perhaps significantly increase the ionization level above that reached by direct field ionization.

Many years ago, it was realized that the relativistic dynamics of single charged particles in plane-wave electromagnetic fields can be solved exactly. Sarachik and Schappert[7] provided a particularly lucid account of the theory, based upon the Hamilton-Jacobi formalism. They discussed at length the motion of an electron that is at rest before the electromagnetic pulse arrives.

In Sec. II of this paper we will discuss the more general solution[8] in which the velocity of the electron is specified at an arbitrary time during the pulse. This solution can then be used to discuss the behavior of photoelectrons that are detached from their parent atoms into a very dilute plasma or the motion of an electron following a scattering event during a laser pulse. In Sec. III we will describe the results of numerical solutions of the relativistic dynamics for some more realistic situations.

II. EXACT SOLUTIONS FOR INDIVIDUAL ELECTRONS IN STRONG PLANAR FIELDS

Neglecting the radiation reaction, the relativistic equations of motion can be solved exactly for electromagnetic pulses that can be described by a vector field A that is just a function of the phase η given by

$$\eta=\omega t-kz \ . \tag{2.1}$$

Note that the z axis has been chosen along the direction of propagation.

Let us impose the initial conditions at $\eta=\eta_0$, when $\mathbf{A}(\eta)=\mathbf{A}_0$. The kinetic momentum is assumed to be

$$\mathbf{p}=\mathbf{p}_0\equiv\mathbf{p}_{0T}+p_{0L}\hat{\mathbf{z}} \tag{2.2}$$

and the canonical momentum is

$$\mathbf{\Pi}=\mathbf{\Pi}_0\equiv\left[\mathbf{p}_{0T}-\frac{e}{c}\mathbf{A}_0\right]+p_{0L}\hat{\mathbf{z}}\ . \tag{2.3}$$

The initial energy is

$$E_0=(p_{0T}^2+p_{0L}^2+m^2c^4)^{1/2}\ . \tag{2.4}$$

We will use the subscripts T and L throughout to indicate transverse and longitudinal components. Note that we have modified the notation of Sarachik and Schappert (SS) by taking the electronic charge to be $-e$ and by writing the vector potential as $A(\eta)$. We will also change the sign of the constant β that appears below so that it becomes positive. The symbol $\hat{\mathbf{z}}$ denotes a unit vector in the z direction.

The general SS solution can be obtained from their Eqs. (2.6) and (2.8) by setting $\alpha=\Pi_{0T}$ and $\beta=E_0/c-p_{0L}$. The kinetic momentum of the electron is given by

$$\mathbf{p}-\mathbf{p}_0=\boldsymbol{\sigma}+\hat{\mathbf{z}}\frac{\boldsymbol{\sigma}\cdot(\boldsymbol{\sigma}+2\mathbf{p}_{0T})}{2\beta}\ , \tag{2.5}$$

where

$$\boldsymbol{\sigma}=\frac{e}{c}[\mathbf{A}(\eta)-\mathbf{A}_0]\ . \tag{2.6}$$

The energy of the electron can then be calculated from

$$E^2=m^2c^4+p^2c^2\ . \tag{2.7}$$

This solution was first derived by Krüger and Bovyn.[8]

A. The motion of preionized electrons

The standard SS solution can be recovered by setting $p_0=0$ and $A_0=0$ to represent the behavior of a free electron which is at rest prior to the arrival of the pulse. We then have

$$\mathbf{p}=\frac{e}{c}\mathbf{A}+\hat{\mathbf{z}}\frac{e^2A^2}{2mc^3} \tag{2.8}$$

and

$$E=mc^2\left[1+\frac{e^2A^2}{2m^2c^4}\right]=\gamma mc^2\ . \tag{2.9}$$

Let us next consider the significance of this solution for pulses with $A(\eta)$ of the form

$$\mathbf{A}(\eta)=A_PP(\eta)[x\delta\cos\eta+y(1-\delta^2)^{1/2}\sin\eta]\ . \tag{2.10}$$

The parameter δ characterizes the polarization, with $\delta=0,\pm1$ giving linear polarization and $\delta=\pm1/\sqrt{2}$ giving circular polarization. $P(\eta)$ is an envelope function which determines the pulse shape and has the value 1 at the peak of the pulse. Following Sarachik and Schappert, we define the dimensional parameter $q=eA_P/mc^2$ to describe the peak field strengths.

For intense fields most of the energy and momentum is associated with motion in the z direction, i.e., along the direction of propagation of the laser. Indeed, since the mass of the electron rises as A^2 and the transverse momentum as A, the velocity of transverse oscillations tends to zero as $1/A_0\rightarrow\infty$. Since p_z is always positive, the electron is carried along with the pulse, and a large time dilation effect is observed as η increases with time much more slowly than ωt. Thus the period of the transverse oscillations increases. The amplitude of these oscillations does not necessarily decrease with increasing A, because of the time dilation effect.

These dilation effects can be computed easily for circularly polarized light, since the longitudinal component of momentum does not oscillate with the field. At the peak of a pulse for which $eA_P\gg mc^2$ the electron's longitudinal velocity is

$$v_z=\frac{p_z}{m\gamma}=c\left[1+4\frac{m^2c^4}{e^2A_P^2}\right]^{-1}=c\left[1+\frac{4}{q^2}\right]^{-1}\ , \tag{2.11}$$

so that

$$\frac{d\eta}{dt}=\omega\left[1-\frac{v_z}{c}\right]\simeq\frac{4\omega}{q^2}\ . \tag{2.12}$$

The period τ and radius ρ of the transverse circular motion are then given by

$$\tau\simeq\frac{\pi}{2\omega}q^2 \tag{2.13}$$

and

$$\rho\simeq\tau\frac{p_T}{m\gamma}\simeq\tau\frac{2c}{q}=\frac{\pi}{\omega}cq=\frac{\lambda q}{2}\ . \tag{2.14}$$

Thus the radius increases indefinitely as q increases, despite the reduction in the transverse velocity!

For noncircular polarization the longitudinal momentum oscillates with a frequency twice that of the transverse motion. It is helpful to introduce a frame R which is moving in the z direction with a velocity equal to the average velocity of the electron, which is given by the right-hand side of Eq. (2.11). In this reference frame the electron executes a figure-eight motion.

Sarachik and Schappert have carefully analyzed the radiation emitted by the electron. They show that the radiation is concentrated around the surface of a cone inclined at an angle $\theta_0=\sqrt{8}/q$ to the z direction. The radiated power per unit solid angle along this cone increases as q^5 and the radiation includes strong components from all harmonics up to the order $n_0=3(1/2q^2)^{3/2}$. Such an intense source of high-order harmonics could have important practical significance if it persists in many-electron systems.

Perhaps the most remarkable feature of the SS solution is that after the pulse has passed the momentum of the electron returns to zero. It has been pointed out[9,10] that this feature could lead to the formation of relatively cold highly ionized plasmas, ideally suited to the production of short-wavelength recombination lasers.

In the remaining sections of this paper we will examine how the various features of this solution are modified as the electron density is raised and inhomogeneities in the radiation field are introduced.

B. The dynamics of photoelectrons

In single-pulse experiments most of the electrons that interact with the laser are created by photoionization during the pulse. For intense lasers incident upon heavy atoms, the outer electrons are detached early in the pulse while the intensity is relatively low. As mentioned in the Introduction, the inner electrons experience the laser as a relatively low-frequency perturbation. Corkum *et al.*[5] have pointed out that the dynamics of electrons that are ionized near the peak of the pulse is very sensitive to the polarization of the light. For linearly polarized light the ionization occurs predominantly during those points in the cycle when the field is greatest. At these times the vector potential is close to zero. On the other hand, when the polarization is circular the magnitudes of the electric field and vector potential do not vary during the cycle. In either case the electron leaves the nucleus with a speed which is small compared to that which it will attain during the subsequent motion.

The final momentum of the photoelectron after the passage of the pulse is obtained by setting $A=0$ in Eqs. (2.5) and (2.6). Thus

$$\mathbf{p}_f=\left[\mathbf{p}_0-\frac{e}{c}\mathbf{A}_0\right]-\hat{\mathbf{z}}\frac{e\,\mathbf{A}_0}{2\beta c}\cdot\left[2\mathbf{p}_{0T}-\frac{e}{c}\mathbf{A}_0\right]. \quad (2.15)$$

For linearly polarized light p_0 and A_0 will be small and $\beta\simeq mc$. Thus the final momentum of the electron is approximately equal to its canonical momentum just after ionization, and will thus also be small. For circularly polarized light, although p_0 will usually be small and β close to mc, A_0 will be large. Thus

$$p_f\approx-\frac{e}{c}A_0+\hat{\mathbf{z}}\frac{e^2A_0^2}{2mc^3}. \quad (2.16)$$

Thus when $eA_0\gg mc^4$, the photoelectrons will be left at highly relativistic velocities, with most of the momentum being along the direction of propagation of the laser.

Corkum *et al.*[5] have observed that the photoelectrons produced at moderate intensities by circularly polarized light have greater residual energy than those produced by linearly polarized light. The above analysis shows that this feature is enhanced in the relativistic limit when the electrons move independently in a plane-wave field. We will show below that this effect is masked in more complex situations.

It is interesting to note that electrons which are freed from their parent ions near the peak of the pulse pick up energy of the order of $e^2A_p^2/4mc^2$ during the first cycle after their release. The acquisition of this energy is not associated with any gradients of the field energy. It should also be noted that there appears to be some ambiguity about the definition of ponderomotive energy in the relativistic limit. Bucksbaum[11] links the ponderomotive energy to the energy of the transverse motion, whereas other authors include the energy associated with the motion along the direction of propagation.

C. Post-collision dynamics of scattered electrons

Suppose an electron which is at rest in a dilute gas before the arrival of the laser pulse undergoes a single collision with an atom, ion, or another electron during the interaction with the laser pulse. Let us denote the change in the electron momentum due to the collision by Δp and the corresponding change in energy by ΔE. We will assume that the duration of the collision is much shorter than the laser period and denote the field vector at the time and place of collision by $\mathbf{A}_0$.

The momentum before collision is obtained by putting $\mathbf{A}=\mathbf{A}_0$ in Eq. (2.9). The momentum after collision then serves as the initial momentum for the post-collision dynamics, which is thus described by Eqs. (2.5)–(2.7) with

$$\mathbf{p}_0=\frac{e}{c}\mathbf{A}_0+\hat{\mathbf{z}}\frac{e^2A_0^2}{2mc^3}+\Delta p \quad (2.17)$$

and

$$\beta=mc-\Delta p_L+\frac{1}{c}\Delta E. \quad (2.18)$$

The residual momentum of the electron after passage of the pulse is then

$$\mathbf{p}_f=\Delta p+\hat{\mathbf{z}}\frac{e\,\mathbf{A}_0}{2c}\cdot\left[\frac{e\,\mathbf{A}_0}{mc^2}-\frac{1}{\beta}\left[2\delta p_T+\frac{e\,\mathbf{A}_0}{c}\right]\right]. \quad (2.19)$$

For most collisions we can assume that $\Delta p\ll mc$ and $\Delta E\ll mc^2$. The residual momentum can then be approximated by

$$\mathbf{p}_f=\Delta p-\hat{\mathbf{z}}\frac{e\,\mathbf{A}_0}{2mc^2}\cdot\left[\Delta p_T+\frac{e\,\mathbf{A}_0}{mc^2}\left[\Delta p_L-\frac{1}{c}\Delta E\right]\right]. \quad (2.20)$$

For linearly polarized light the energy of the oscillating electron varies significantly, and collisions are more likely when the velocity is low, that is, for small values of A_0. Thus for almost all collisions the residual momentum of the electron will equal the momentum transferred to the collision.

Electron-ion collisions that result in inner-shell excitation or ionization are of special interest. Since Δp and ΔE are large in such collisions they can lead to a significant increase in the residual energy of the scattered electron. Furthermore, following inner-shell ionization the emitted electron will in general emerge with a velocity that is not in phase with the laser in the manner expressed in Eq. (2.8). Thus its residual momentum will also be large. Inner-shell ionization during the laser pulse will then lead to two energetic electrons and will result in significant absorption of energy from the field.

III. NUMERICAL SIMULATIONS OF RELATIVISTIC ELECTRON DYNAMICS

In this chapter we study two generalizations of the analytic theory described in Sec. II. For high-density plasmas the motion of the electrons produces strong space-charge forces which modify the electron dynamics and the propagation of the pulse. These effects can only be fully analyzed through a multielectron simulation and we have initiated such studies. Initial results suggest that the results of many-electron simulations will be much

more difficult to interpret. Thus we believe it will be very helpful to perform some single-particle simulations in which the space-charge effects are represented by a potential and the effects of the electron motion upon laser propagation are neglected. Such studies are described in Sec. III A. These calculations follow the example of Kyrala[12] who has used a similar approach to study the effect of the Coulomb interaction with the nucleus.

The creation of very intense fields can only be accomplished currently through tight focusing of a laser beam. There is also evidence that narrow filaments will form in intense beams, leading to spatial inhomogeneities. It will therefore be necessary to study the effects of spatial variations in the laser intensity. In Sec. III B we discuss a simple model which illustrates the effect of such variations on the electron dynamics. Again we do not study the effects of the spatial variations of the laser intensity on the propagation of the beam, and will postpone the presentation of a self-consistent solution for electron dynamics and laser propagation to a later publication.

In performing these calculations we have used atomic units, in which $e=m_e=\hbar=1$ and $c=137.07$. As an aid to the reader we will retain these fundamental quantities in the equations of this section, but all of the figures are in atomic units.

A. A simple model of space-charge forces

We saw in Sec. II that irradiation by an intense laser pulse propels free electrons at high average velocity in the direction of propagation of the laser. In a dense plasma this leads to a separation of charge and to the growth of electrostatic forces that might cause significant modification of the electron dynamics. To provide a simple model for this effect within the plane-wave pulse approximation, we will add a harmonic restoring force in the direction of propagation of the laser,

$$\mathbf{F}=-m\omega_p^2\mathbf{z} \ . \tag{3.1}$$

We will refer to ω_p as the plasma frequency, although its role in our calculation is only through its control of the strength of the restoring force.

The results presented in this chapter were all obtained through the numerical solution of the relativistic Newton-Lorentz equation

$$\frac{d}{dt}\mathbf{P}=-e\mathbf{E}-\frac{e}{c}\mathbf{v}\times\mathbf{B}-m\omega_p^2\mathbf{z} \ . \tag{3.2}$$

The variable-step Runge-Kutta technique was found to be more efficient than the Boris and Adams-Bashforth methods. The code was first tested by setting $\omega_p=0$ and comparing against the predictions of the Sarachik-Schappert solution. Figures 1(a) and 1(b) show the time variation of the transverse (p_x) and longitudinal (p_z) momenta for an electron, initially at rest, in a plane-wave linearly polarized field with a maximum field strength of 100 a.u. (5.14×10^{11} V/cm), corresponding to an intensity of 3.5×10^{20} W/cm^2 at a frequency $\omega=0.18$ a.u., which is close to that of a Kr:F laser. This laser frequency will be used throughout this chapter. The results shown in Fig. 1 are in excellent agreement with the predictions of Eq. (2.8). The maximum electron energy is 4.7 MeV.

The introduction of a weak restoring force leads to results, as shown in Figs. 2(a) and 2(b), which were obtained with $\omega_p=0.01$. Note that the transverse component of the canonical momentum remains zero so that

$$\mathbf{P}_T(\eta)=\frac{e}{c}\mathbf{A}(\eta) \ . \tag{3.3}$$

Thus the transverse kinetic momentum is modified only because of changes in η, and oscillates between the same limits as in Fig. 1(a). The effect of time dilation is apparent near $\omega t=0$ and 80π, and of time contraction near $\omega t=40\pi$ in both p_x and p_z. The maximum values of momentum and energy are changed very little from the values found with $\omega_p=0$. However, as the value of ω_p is raised further, as shown in Figs. 3(a) and 3(b), the maximum in the longitudinal momentum is increased significantly and the peak energy reaches values in excess of 25 MeV.

In performing these integrations we found it necessary to impose strict limits on the integration error tolerated in each cycle. This suggests that the dynamics might be very sensitive to small changes in the initial conditions,

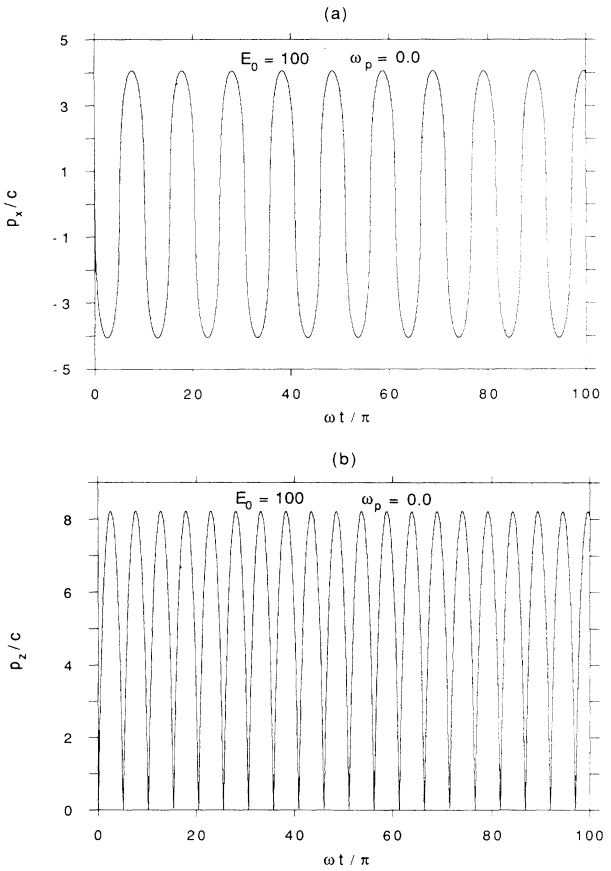

FIG. 1. Time dependence of the (a) transverse and (b) longitudinal momentum for an electron under the influence of a linearly polarized laser field of constant amplitude 100 a.u. and frequency 0.18 a.u.

which was confirmed by the results shown in Fig. 4. This figure shows the time dependence of the difference in the momentum of two electrons which have initial velocities of 0 and 0.1 a.u. The difference in the initial momentum corresponds to an energy difference of less than 0.2 eV. However, the difference in energy of the two electrons after interacting with the field for 50 optical cycles is of the order of 5 MeV. This extreme sensitivity to the initial conditions is characteristic of chaotic motion. It appears that the introduction of relativistic dynamics has introduced nonlinearities which transform the periodic motion of a driven harmonic oscillator into irregular motion.

Although calculations with a fixed laser intensity may approximate the behavior of an electron that is ionized during a long pulse, it is more interesting to consider pulses in which the laser intensity varies with time. Let us next consider the motion of an ambient electron that is at rest before the arrival of a short pulse, with a vector potential defined by

$$E_x(\eta)=\begin{cases}0 & \text{if } \eta<0\\ E_0\sin\eta\sin^2(\eta/N) & \text{if } 0<\eta<N\pi\\ 0 & \text{if } \eta>N\pi\ .\end{cases} \tag{3.4}$$

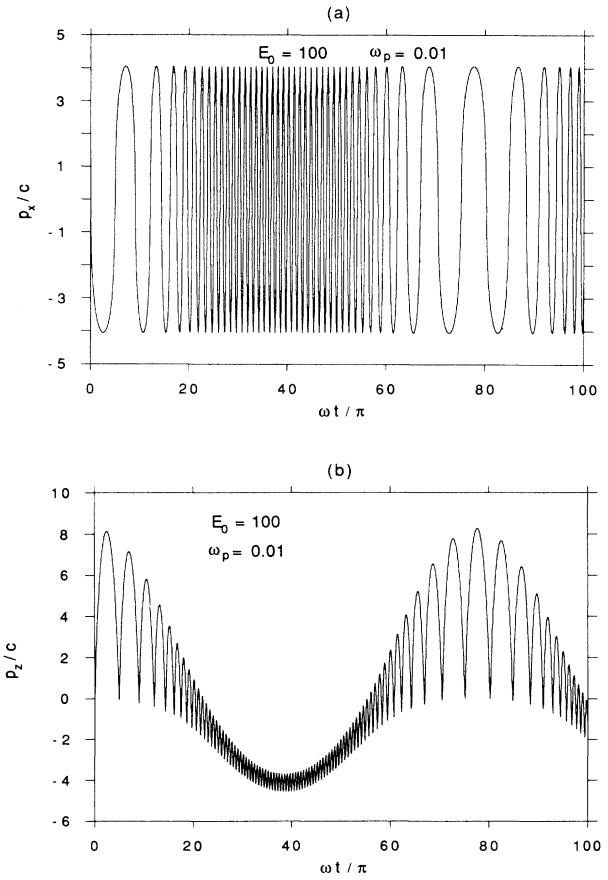

FIG. 2. Same as Fig. 1, except for the presence of a harmonic restoring force with a strength equivalent to a nonrelativistic plasma frequency of 0.01 a.u.

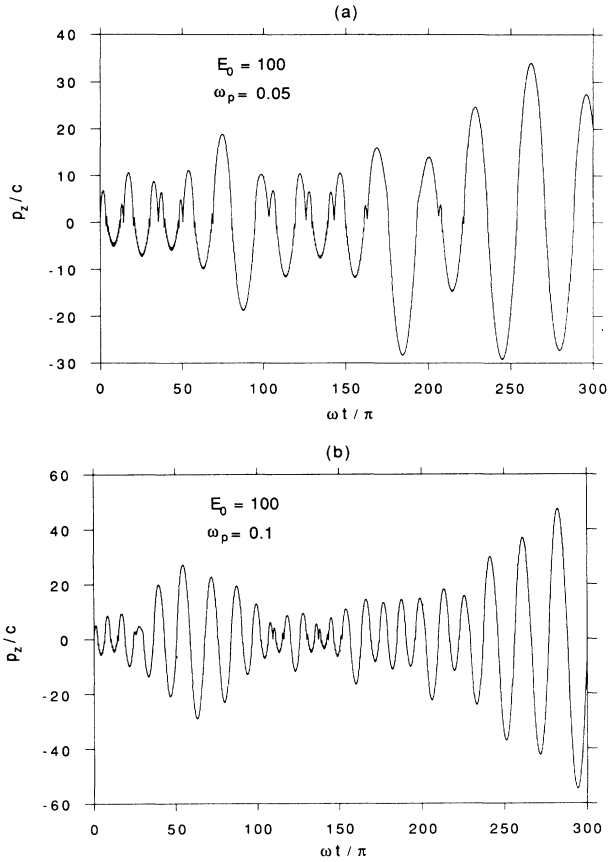

FIG. 3. Same as Fig. 2(b), but with a plasma frequency of (a) 0.05 a.u. and (b) 0.1 a.u.

The time variation of the electric field experienced by the electron with $N=100$ is shown in Figs. 5(a) and 5(b). For small values of ω_p, as used in Fig. 5(a), the time dilation effect is large and the electron interacts with the field for much longer than the time that it takes the pulse to pass a fixed point in space. At larger values of ω_p the electron

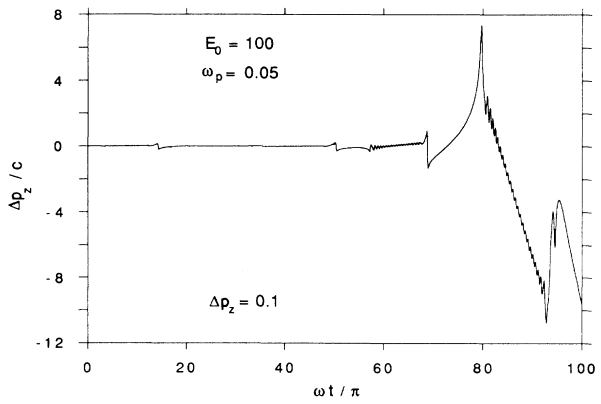

FIG. 4. Time dependence of the difference in the longitudinal momentum of two electrons moving under the conditions of Fig. 3(a) with initial momenta p_z of 0 and 0.1 a.u.

is not carried along by the pulse and the interaction time is close to the pulse length.

Figures 6(a) and 6(b) show the time variation of the longitudinal momentum for two values of ω_p such that $\omega_p T \ll 2\pi$, where $T\ (=N\pi/\omega)$ is the pulse length. The amplitude of the oscillations in p_z rises and falls with the laser intensity, and the residual momentum of the electron is relatively small. Figure 7 corresponds to a value of $\omega_p T/2\pi$ equal to 1.4 and shows that the residual momentum can be larger when the frequency associated with the laser intensity envelope matches the plasma frequency.

As ω_p is raised further the residual momentum becomes small again, as shown in Figs. 8(a) and 8(b). Note that in this region, for which

$$\frac{2\omega}{N} \ll \omega_p \ll 2\omega \ , \tag{3.5}$$

the maximum value of p_z near the peak of the pulse is relatively insensitive to the value of ω_p, but is significantly lower than the value obtained with $\omega_p = 0$. Figures 9(a) and 9(b) suggest that this peak value is also insensitive to the pulse length. Figure 9(a) corresponds to a pulse with a "sine-square" envelope of double length, whereas Fig. 9(b) was obtained by inserting a 100π segment of constant field intensity in the center of the 100π sine-square pulse.

A second resonance region is found with ω_p between 0.2 and 0.4, as illustrated in Figs. 10(a) and 10(b). During the interaction with the pulse the longitudinal momen-

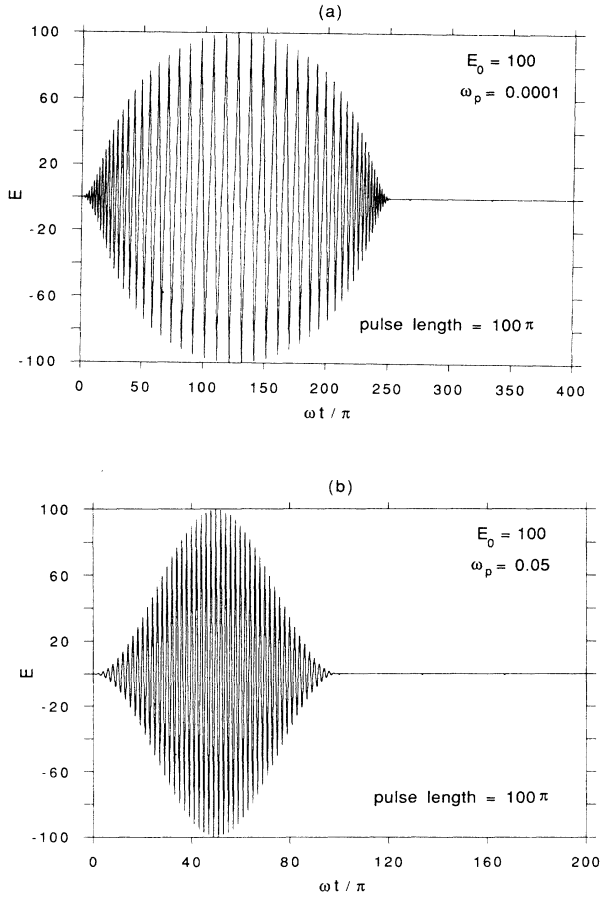

FIG. 5. Time dependence of the field experienced by electrons in the laser field described by Eq. (3.4) with $E_0 = 100$ a.u. and $N = 100$, with (a) $\omega_p = 10^{-4}$ a.u. and (b) $\omega_p = 0.05$ a.u.

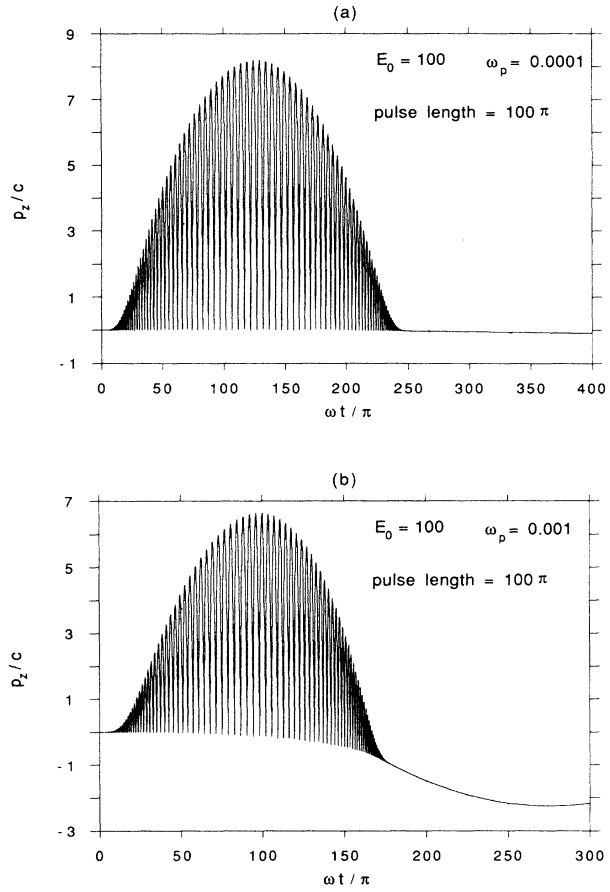

FIG. 6. Time dependence of the longitudinal momentum for the shaped pulse of Fig. 5 with (a) $\omega_p = 10^{-4}$ a.u. and (b) $\omega_p = 10^{-3}$ a.u.

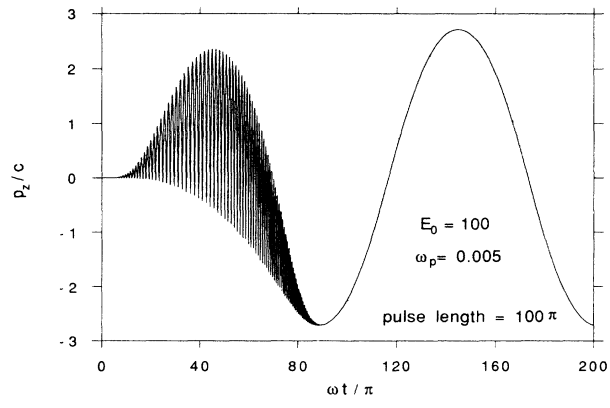

FIG. 7. Same as Fig. 6, but with $\omega_p = 0.005$ a.u.

tum exceeds the value obtained with $\omega_p=0$, and the residual value after the passage of the pulse is large. At higher values of ω_p the residual momentum is again very small, as shown in Fig. 11. However, propagation at the densities required to produce such high values of ω_p will only be possible at very high laser intensity.

The dependence of the residual momentum upon ω_p is shown in Fig. 12. For ω_p between 0.03 and 0.20, ambient electrons, which are at rest before the arrival of the pulse, return to a low velocity after the passage of the pulse, as was found by Sarachik and Schappert for $\omega_p=0$. We do not yet fully understand the fine structure in the upper resonance region.

In Fig. 13 we show the dependence of the maximum value of p_z upon the peak intensity in the pulse for $\omega_p=0.05$ and $\omega T=100\pi$. At small values of E_0, for which $q<1$, the peak value is proportional to E_0^2, as is expected for nonrelativistic dynamics. At higher values of E_0 the maximum momentum rises more slowly, approximately proportional to E_0. Thus adiabatic switching of the field significantly reduces the peak momentum and energy associated with the quiver motion of electrons which are at rest prior to the arrival of the pulse.

The reduction in the magnitude of the longitudinal momentum due to adiabatic switching is even more dramatic for circularly polarized light. Figures 14(a) and 14(b) show results for a maximum field strength of 70.7 a.u., which produces the same average laser intensity as the linearly polarized waves with a maximum field strength of 100 a.u. With a constant field amplitude the momentum reaches values in excess of $20mc$, corresponding to energies over 10 MeV. However, when the field is turned on over 25 optical cycles the maximum value of the longitudinal momentum is three orders of magnitude smaller. We will try to explain this behavior in Sec. IV.

B. Effects of space-charge forces on photoelectrons

In Sec. II B we pointed out that for linearly polarized light most photoelectrons are created with relatively low velocities at times and positions such that the vector potential is also small, and argued that the subsequent dynamics of photoelectrons is therefore similar to that of ambient electrons that are at rest before the arrival of the pulse. This leads to small residual momenta for most photoelectrons ionized by linearly polarized lasers in very dilute gases.

When there are substantial space-charge forces this similarity is destroyed, since the points, in time and space, at which the longitudinal momentum is zero do not correspond to the points where the vector potential is

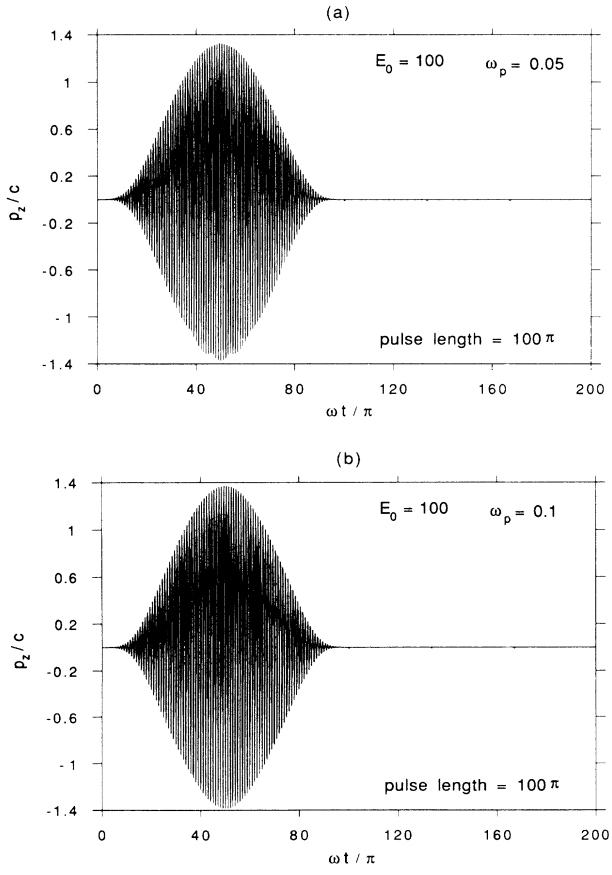

FIG. 8. Same as Fig. 6, but with (a) $\omega_p=0.05$ a.u. and (b) $\omega_p=0.1$ a.u.

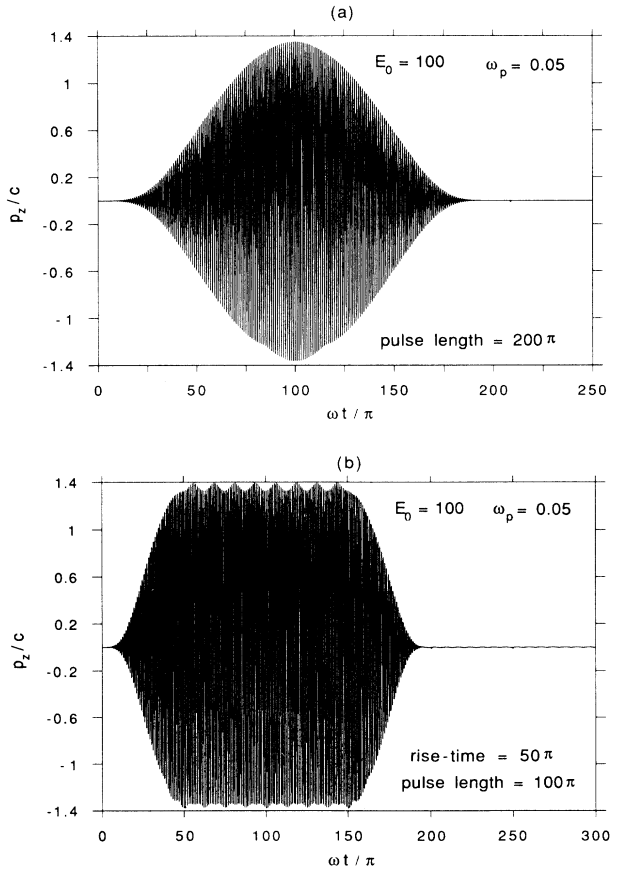

FIG. 9. Same as Fig. 8(a) but with (a) a longer pulse with $N=200$ and (b) a constant field amplitude portion in the center of the pulse used in Fig. 8(a).

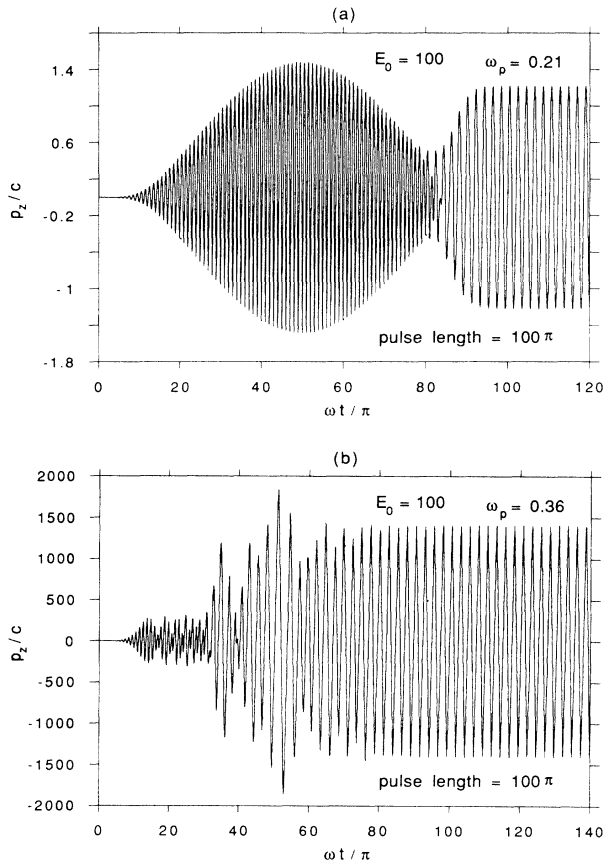

FIG. 10 Same as Fig. 6, but with (a) $\omega_p=0.21$ a.u. and (b) $\omega_p=0.36$ a.u. Note that the laser frequency is 0.18 a.u.

zero. Thus there is no reason to expect that photoelectrons which are created near the peak of an intense laser pulse will return most of their quiver energy to the field. To check this we followed the motion of an electron created with zero velocity at the origin half-way through the pulse described by Eq. (3.3). The resulting longitudinal momentum is shown in Fig. 15, and a large residual value is obtained. The formation of a cool overionized plasma will be hindered by this effect.

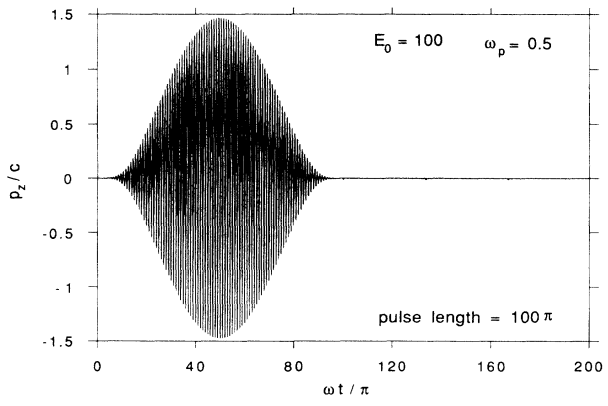

FIG. 11. Same as Fig. 6, but with $\omega_p=0.5$.

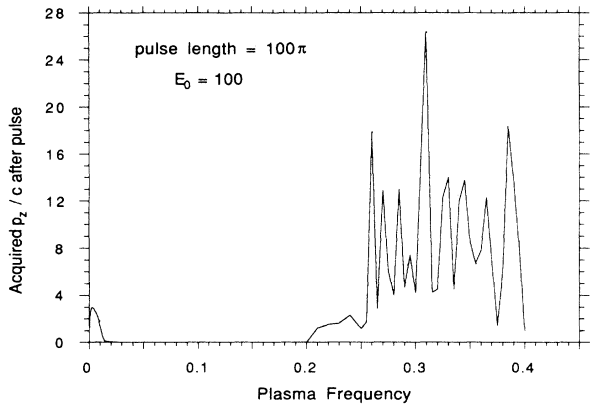

FIG. 12. Residual longitudinal momentum of the electron following the laser pulse of 50-cycle duration with maximum field amplitude of 100 a.u. as a function of the strength of the harmonic restoring force.

C. Effects of spatial variations in laser intensity

Let us suppose that the laser is polarized along the x axis, and that the field strength varies with x as

$$E(x)\propto\exp\left[-\frac{x^2}{s^2}\right]. \tag{3.6}$$

We will refer to the scale length s as the spot size.

Let us first suppose that one can create an intense beam with a relatively large spot size of $5\times10^4 a_0$, which corresponds to 2.6 μm or 10.7λ, with a pulse length of 25 optical cycles (20 fsec). The transverse motion of an electron which is initially at rest at the center of the beam is shown in Figs. 16(a) and 16(b). The maximum amplitude of the oscillations during the pulse is approximately $6000a_0$ or 1.2λ. This value can exceed λ only because of the time dilation effect, since its speed must be less than c and the transverse oscillations are in phase with the field. Note that the maximum value of p_x/c is close to the value of 4.06 expected for oscillation at the peak intensity

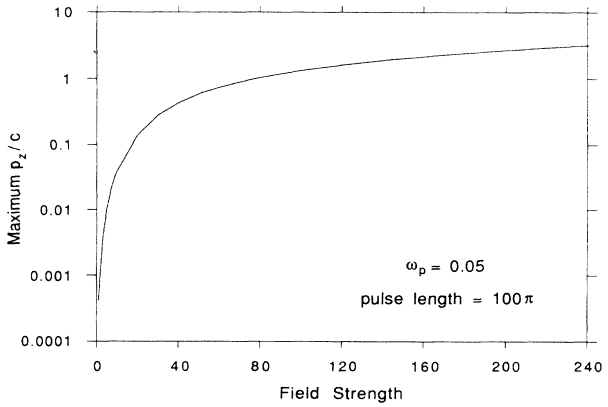

FIG. 13. Maximum value of the longitudinal momentum attained during a 50-cycle pulse with $\omega=0.18$ and $\omega_p=0.05$, as a function of the peak field strength.

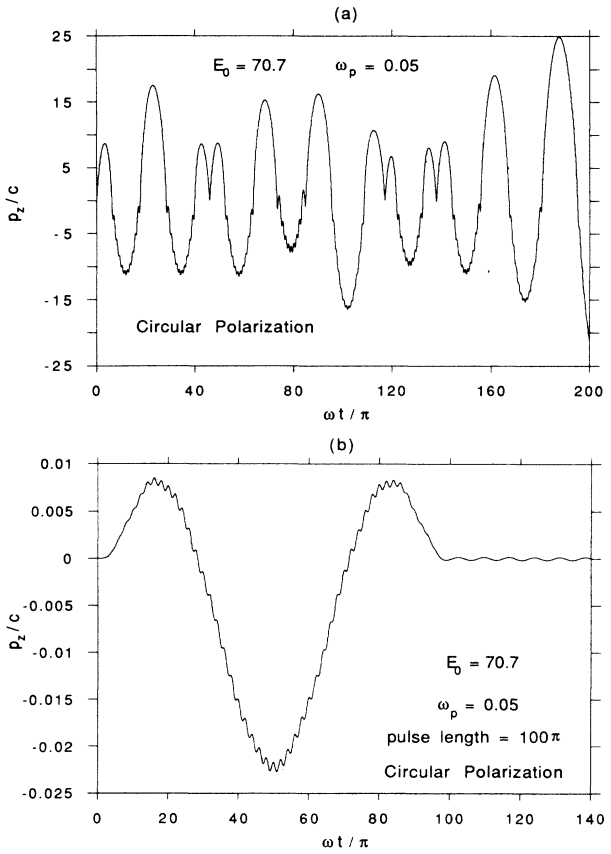

FIG. 14. Time dependence of the longitudinal momentum for an electron in a circularly polarized laser of peak amplitude 70.7 with $\omega_p = 0.05$: (a) for a laser of constant amplitude; (b) for a shaped pulse of length 50 cycles.

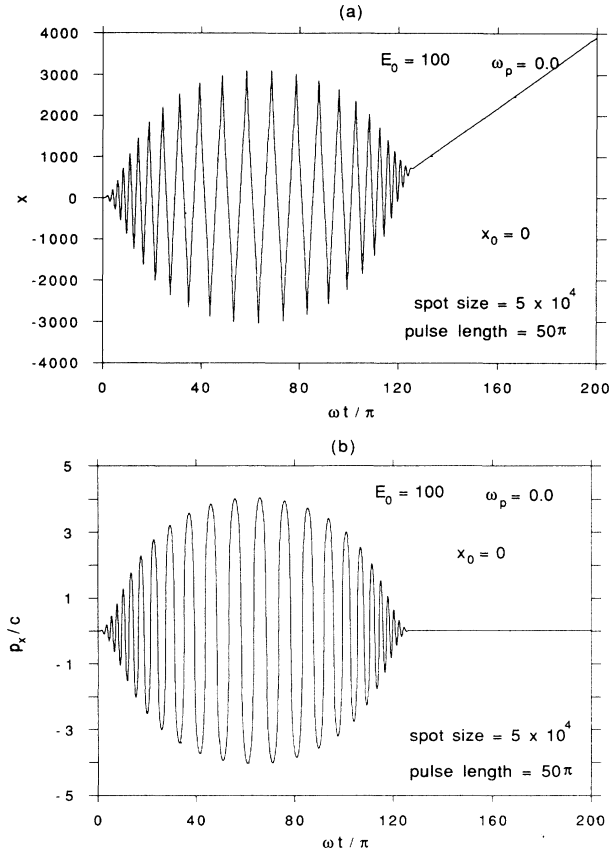

FIG. 16. Transverse motion of an electron initially at rest on the axis of a linearly polarized laser beam of radius 5×10^4 a.u. and 25-cycle pulse duration with peak field of 100 a.u.: (a) position coordinate (in a.u.); (b) momentum.

and that the residual momentum is small. The longitudinal momentum, shown in Fig. 17, is similar to that found with a spatially uniform field. Very different results are found when the electron is started away from the beam center. As can be seen in Figs. 18(a) and 18(b) the electron is ejected from the beam with a large value of both p_x and p_z.

When the spot size is reduced, even electrons that begin at the center of the beam are ejected at high velocity, as shown in Figs. 19(a) and 19(b). It is clear from these two calculations that the dependence of the components of the residual momentum upon E_0 is neither linear nor quadratic. Photoelectrons which are released by the ions

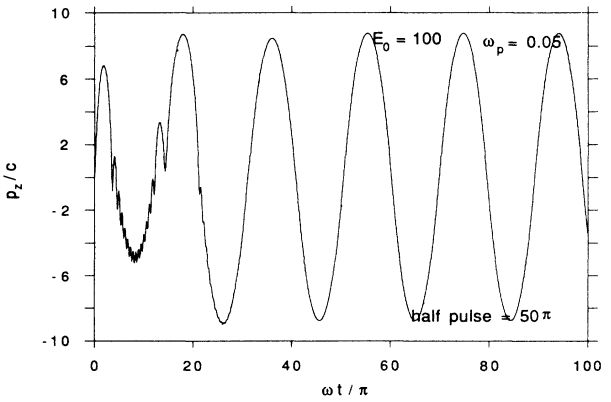

FIG. 15. Time dependence of the longitudinal momentum for an electron which is created at the center of a 50-cycle pulse of a linearly polarized laser with peak field strength of 100 a.u. and $\omega_p = 0.05$.

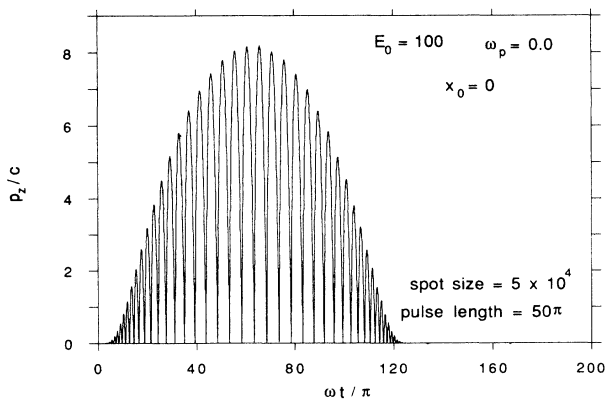

FIG. 17. Longitudinal momentum corresponding to the transverse motion shown in Fig. 16.

near the center of the pulse are ejected more rapidly, as shown in Figs. 20(a) and 20(b). The spot size used in these latter calculations is approximately 2λ.

It is likely that filaments will form in the focal regions of very intense lasers. The inhomogeneities associated with these filaments will also increase the residual momentum of electrons ionized therein.

Since the major purpose of this paper is to provide numerical results for simple systems, in the hope of stimulating analytical study, we do not present results for systems with both lateral variations in intensity and transverse space-charge forces. The introduction of transverse space-charge forces should restrain and expulsion of electrons, but will not necessarily reduce the residual momentum of the electrons. The study of lateral variations in electron density and their effects on the refractive index and laser propagation will form an important part of our future studies.

IV. ANALYSIS OF THE ONE-DIMENSIONAL MODEL

The model introduced in Sec. III A is essentially one dimensional since the transverse components of the canonical momentum are constant throughout the motion. The longitudinal momentum is given by the equation

$$\frac{d}{dt}p_z + m\omega_p^2 z = -\frac{e}{c}\mathbf{v}\times\mathbf{B} \ . \tag{4.1}$$

Writing $\mathbf{B}=\nabla\times\mathbf{A}$, replacing $\mathbf{v}$ by $e\,\mathbf{A}/m\gamma c$, and using

$$\frac{d\,\mathbf{A}}{dt} = \left[1-\frac{v_z}{c}\right]\frac{\partial\,\mathbf{A}}{\partial t} = -c\left[1-\frac{v_z}{c}\right]\frac{\partial\,\mathbf{A}}{\partial z} \ , \tag{4.2}$$

the equation of motion becomes

$$\frac{d}{dt}p_z + m\omega_p^2 z = \frac{e^2}{2mc^3}\frac{1}{\gamma(1-v_{z/c})}\frac{d}{dt}(A^2) \ . \tag{4.3}$$

The simplicity of the solution for $\omega_p=0$ arises because

$$\gamma\left[1-\frac{v_z}{c}\right]=1 \ . \tag{4.4}$$

However, when $\omega_p\neq 0$ this relationship between v_z and γ does not hold. The magnitude of the product on the left-hand side of Eq. (4.4) provides the key to understanding the longitudinal motion. Small values of v_z/c are not necessarily accompanied by small values of v_T/c; $\gamma(1-v_z/c)$ is then greater than 1 and $|dp_z/dt|$ is re-

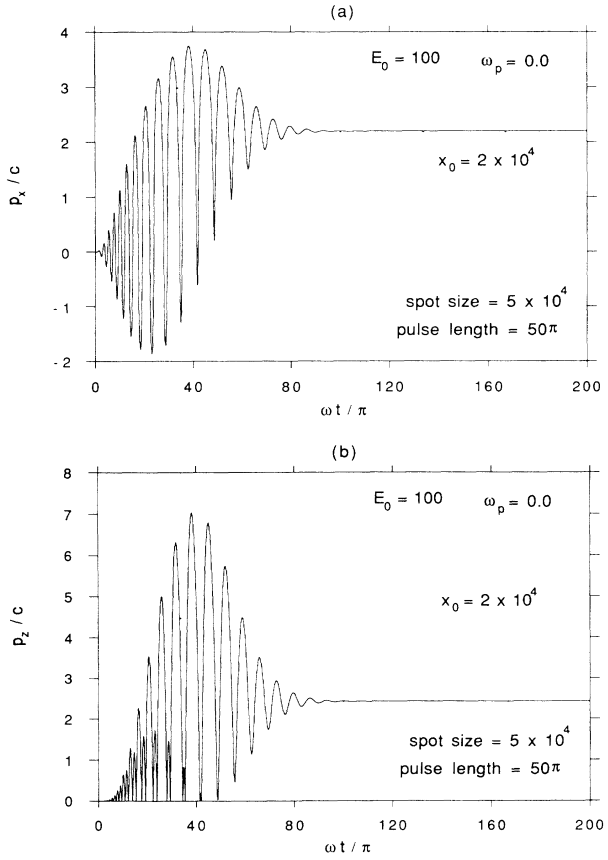

FIG. 18. Time dependence of the momentum of an electron in the laser pulse of Fig. 16 which begins at rest at a position 2×10^4 a.u. off the laser beam axis: (a) transverse momentum; (b) longitudinal momentum.

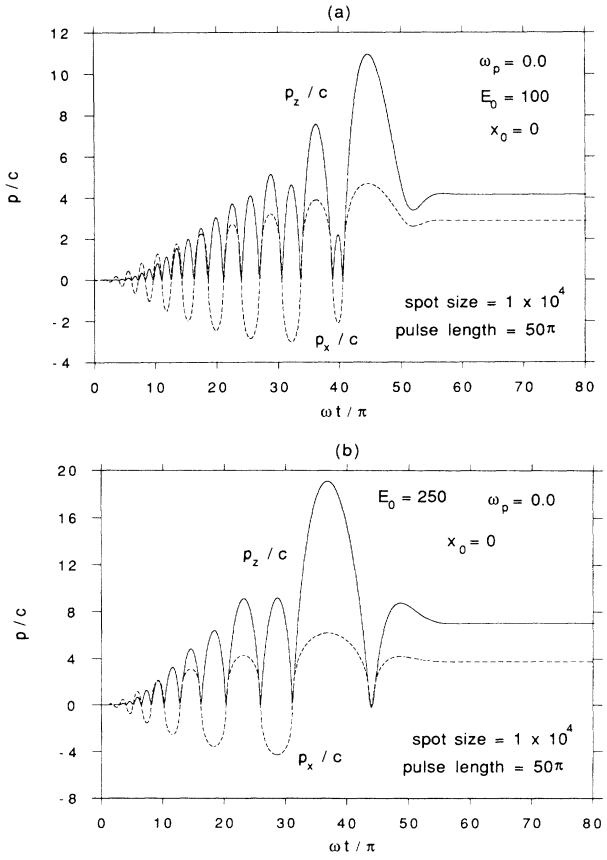

FIG. 19. Transverse and longitudinal momenta for an electron which starts at rest on the axis of a narrow laser beam of radius 1×10^4 a.u. for a peak field strength of (a) 100 a.u. and (b) 250 a.u.

duced. This leads to the reduction of the magnitude of the oscillations in p_z during the adiabatically switched pulses as seen in Figs. 7–9, 11, and 14(b). For circularly polarized light A^2 varies slowly with time and the oscillations in p_z are very small.

When v_z approaches c and exceeds v_T, $\gamma(1-v_z/c)$ is then close to 1 and the full effects of time dilation are seen. The phase changes induced by the space-charge force can then lead to increases in the quiver energy.

The nonlinearity of Eq. (4.3) can perhaps be best illustrated through the contrast between Figs. 3(a) and 9(b), which are both obtained with $\omega_p=0.05$ and $E_0=100$. The quasiperiodic motion observed in the center portion of Fig. 3(a) and the irregular motion seen in Fig. 9(b) satisfy the same equation of motion, and thus the difference must be due to the initial conditions.

The nature of the dynamics can be probed through a phase-space map as shown in Fig. 21. Equation (4.3) is solved for a linearly polarized plane wave of constant amplitude with $E_0=100$ and $\omega_p=0.05$, and the values of z and p_z are recorded whenever the phase η is an integral multiple of 2π, so that $A(\eta)=0$. Several trajectories are shown, each starting with $z=0$, with various initial values of p_z. When $p_z(0)$ is between two critical values, which are approximately $-0.25c$ and $-3.7c$, the motion is quasiperiodic. For values outside this range the motion is chaotic. At the center of the regular region there is a

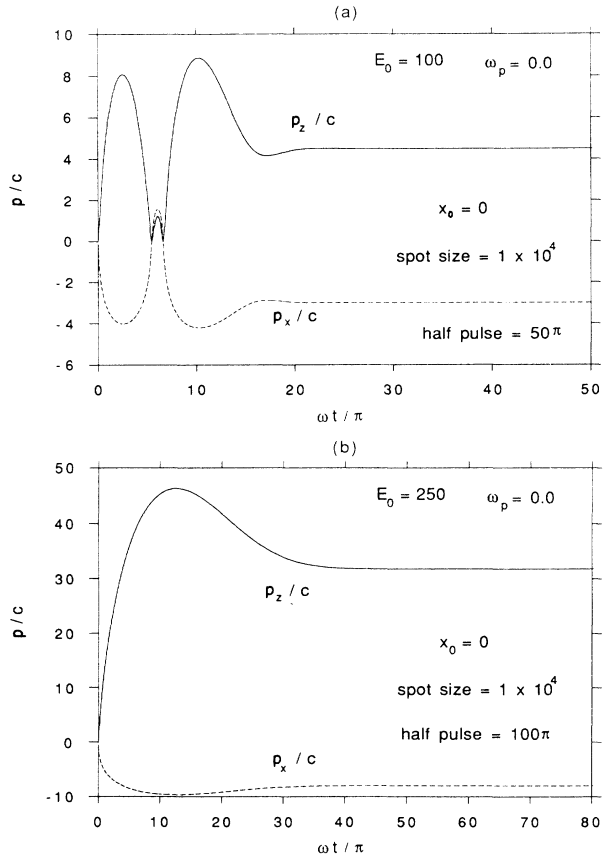

FIG. 20. Same as Fig. 19, but for electrons born at rest at the center of a pulse of length 50 cycles.

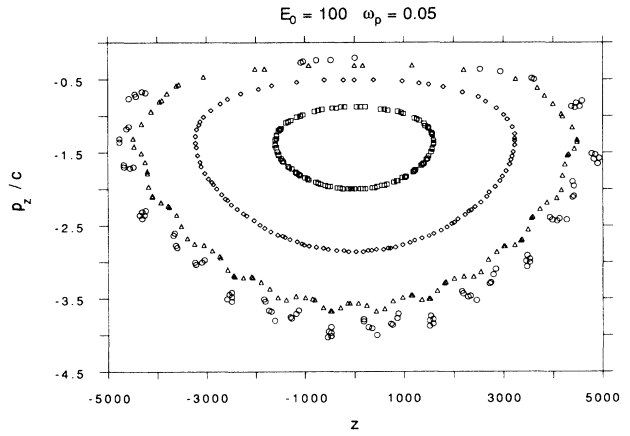

FIG. 21. Phase-space portraits over 100 cycles, as described in the text, for electrons with different initial momenta in a linearly polarized laser field of constant amplitude 100 a.u. with $\omega_p=0.05$: □, $p_{z0}=2.0c$, $p_{z0}=-0.5c$; △, $p_{z0}=0.3c$; and ○, $p_{z0}=-0.2c$.

periodic orbit with $z(0)=0$ and $p_z(0)\approx-1.36$. This is the orbit that is attained when the amplitude of the electromagnetic wave is increased adiabatically. The pulse lengths of 50 and 100 cycles used in generating Figs. 8(a), 9(a), and 9(b) are sufficiently long that the motion is close to the adiabatic limit and the oscillations in p_z near the center of the pulse are between values close to $\pm1.36c$.

The difference in the character of a regular and irregular orbit can be seen by comparing Fig. 22(a), obtained with $p_z(0)=-0.3c$ to Fig. 22(b), for which $p_z(0)=-0.2c$. The regular motion leads to points which form a single closed contour in phase space. During the early portion of the irregular motion there is some clustering around a single contour, but at later times the motion breaks away and the magnitude of p_z increases substantially. The duration of the motion shown in Figs. 22(a) and 22(b) is 400 cycles.

It is especially significant that the regular region does not intersect the axis along which $p_z=0$. Thus all photoelectrons that emerge from ions with nonrelativistic velocities ($v\lesssim0.2c$) when $A(\eta)\approx0$ follow irregular trajectories. Very few photoelectrons are freed at other times during the optical cycle. Electrons that are launched into irregular trajectories during a laser pulse will not return to rest as the laser intensity declines. They will either be ejected from the focal region at high velocity or, if trapped by the space-charge forces, will form a very hot residual plasma.

V. CONCLUSIONS

In this paper we have presented a selection of many interesting results that emerged from our single-particle simulations of relativistic dynamics. Most of the simulations were performed with plane-wave pulses so that the results are functions of only two variables, z and t (or z and η). The one-dimensional harmonic oscillator model of space-charge forces was chosen because the nonrelativistic dynamics can be calculated analytically. Howev-

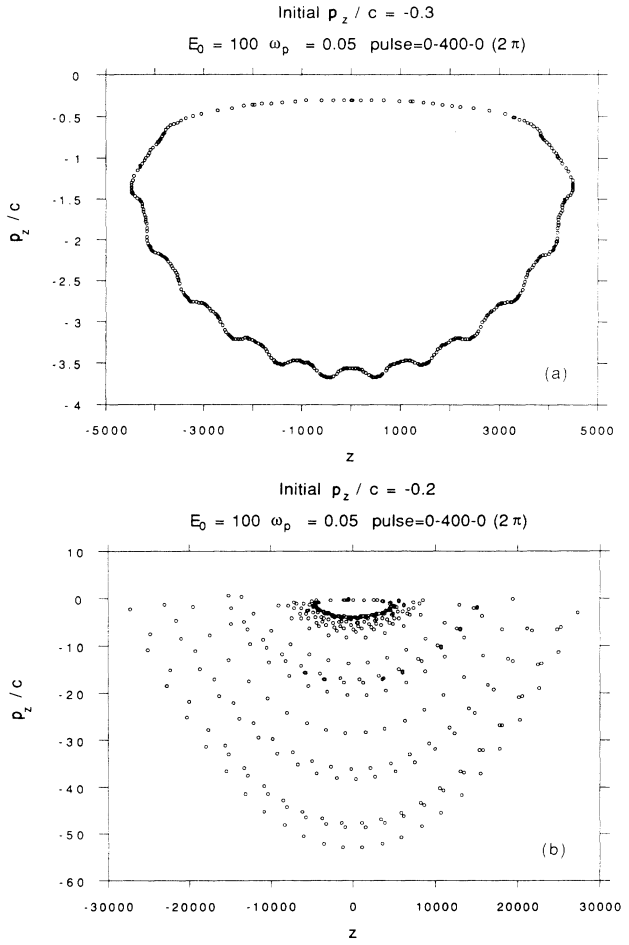

FIG. 22. Phase-space portraits over 400 cycles for (a) a regular orbit with $p_{z0}=-0.3c$ and (b) an irregular orbit with $p_{z0}=-0.2c$.

er, we have so far been unable to obtain a similar solution in the relativistic regime.

The phase-space portraits discussed in Sec. IV provide an explanation for the very different behavior of electrons that are at rest before the arrival of a shaped pulse and electrons which are released into the influence of a time-independent electromagnetic field. Even for pulses as short as 2–3 optical cycles, the continuous increase and decrease in the laser amplitude can lead to significant reductions in the momentum of the quivering electrons. However, when an electron emerges from an ion when the laser amplitude is close to its peak, the resulting mismatch between the phase of the electromagnetic field and the subsequent oscillations of the photoelectron can lead to irregular motion with very high momentum.

When the space-charge fields are large, the results of Sec. IV suggest that almost all photoelectrons that are released at high field intensities execute irregular high-energy orbits, irrespective of the polarization of the laser, whereas for low-density plasma linear polarization usually leads to orbits with low residual energy. For electrons that are ionized through collisions, there is a possibility that the momentum immediately after ionization may place the electron in a regular orbit, but most secondary electrons will also enter irregular trajectories.

The rapid post-ionization acceleration has an important effect on the threshold behavior of cross sections of collisions in intense fields. Despite the fact that the freed electron must enter an orbit with very high energy, most of this energy is supplied by the field. Although the quiver energy effectively raises the threshold for collisional ionization, the quiver energy is gained from the laser field during the first cycle after ionization, and does not have to be supplied by the colliding particle. When the time of the collision is very short, compared with the laser period, the ionization cross section will be close to that found with a dc external field. Since almost all of the outer electrons will have been stripped from the ions during the growth of the field, most of the interesting processes such as inner-shell ionization and pair production have very short time scales and relatively high threshold energies. The cross sections describing the electron release can then be approximated fairly well by the field-free cross sections.

With respect to the physics of relativistic laser-produced plasmas, the results of these numerical experiments must be checked by multiparticle simulations with a consistent treatment of electron dynamics and laser propagation. In the meantime we can make the following preliminary conclusions.

(i) The production of electrons with velocities sufficiently high to induce nuclear reactions through collisions with ionic nuclei is not seriously hindered by space-charge effects.

(ii) The formation of cold overionized plasmas suitable for short-wavelength recombination lasers may be more difficult than is suggested by earlier analyses, since space-charge effects and spatial variations in laser intensity both increase the energy of the residual electrons. The low temperatures required for recombination lasers must then be attained through rapid cooling of the plasma after the pulse has passed.

ACKNOWLEDGMENTS

This work was performed under the auspices of the U.S. Department of Energy by Lawrence Livermore National Laboratory under Contract No. W-7405-Eng-48.

[1]T. S. Luk, T. Graber, H. Jara, V. Johann, and C. K. Rhodes, J. Opt. Soc. Am. B **4**, 847 (1987); A. McPherson, G. Gibson, H. Jara, V. Johann, T. S. Luk, I. A. McIntyre, K. Boyer, and C. K. Rhodes, *ibid.* **4**, 595 (1987).

[2]J. A. Cobble, G. A. Kyrala, A. A. Hauer, A. J. Taylor, C. C. Gomez, N. D. Delameter, and G. T. Schappert, Phys. Rev. A **39**, 454 (1989).

[3]M. M. Murnane, H. C. Kapteyn, and R. W. Falcone, Phys.

Rev. Lett. **62**, 155 (1989); C. H. Nam, W. Tighe, S. Suckewer, J. F. Seely, V. Feldman, and L. A. Woltz, *ibid.* **59**, 2427 (1987).

[4]L. D. Landau and E. M. Lifshitz, *Quantum Mechanics* (Pergamon, Oxford, England, 1965), p. 276.

[5]P. B. Corkum, N. H. Burnett, and F. Bruenel, Phys. Rev. Lett. **62**, 1259 (1989).

[6]K. Boyer, T. S. Luk, and C. K. Rhodes, Phys. Rev. Lett. **60**, 557 (1988).

[7]E. S. Sarachik and G. T. Schappert, Phys. Rev. D **1**, 2738 (1970).

[8]J. Kruger and M. Bovyn, J. Phys. A **9**, 1841 (1976).

[9]J. Peyraud and N. Peyraud, J. Appl. Phys. **43**, 2993 (1972).

[10]N. H. Burnett and P. B. Corkum, J. Opt. Soc. Am. B **6**, 1195 (1989).

[11]P. H. Bucksbaum, in *Proceedings of the NATO Advanced Study Institute on Atoms in Strong Laser Fields, Kos, 1988* (Plenum, New York, 1989).

[12]G. A. Kyrala, J. Opt. Soc. Am. B **4**, 731 (1987).